Variations of total electron content during geomagnetic disturbances: A model/observation comparison

G. Lu,[1] X. Pi,[2] A. D. Richmond,[1] and R. G. Roble[1]

[1] High Altitude Observatory, National Center for Atmospheric Research

[2] Jet Propulsion Laboratory, California Institute of Technology

Abstract. This paper studies the ionospheric response to a major geomagnetic storm of October 18-19, 1995, using the thermosphere-ionosphere electrodynamics general circulation model (TIE-GCM) simulations and the global ionospheric maps (GIM) of total electron content (TEC) observations from the Global Positioning System (GPS) worldwide network. The TIE-GCM results, which utilize the realistic time-dependent ionospheric convection and auroral precipitation derived from the assimilative mapping of ionospheric electrodynamics (AMIE) procedure as the inputs at the upper boundary, shows a good agreement with the GPS-GIM in terms of simulating storm-time TEC disturbances over the polar regions as well as variations in hemisphere-integrated TEC. The model simulation indicates that the increase of electron density, especially in the high-latitude E and lower F regions below 200 km, is directly related to the magnetospheric energy inputs (through Joule heating and auroral precipitation) to the ionosphere. A good correlation is found between the percent increase in TEC and auroral precipitation during the main phase of the storm. The simulation also shows that the decrease of TEC, on the other hand, is mainly due to the increase in O_2 and N_2 in the upper F region above 200 km. During the recovery phase, both

TIE-GCM and GPS-GIM reveal a distinct hemispheric asymmetry in the hemisphere-integrated TEC, with a 2070 decrease in the southern (summer-like) hemisphere and a 30% increase in the northern (winter-like) hemisphere.

Introduction

During geomagnetic disturbances, such as geomagnetic storms and substorms, the energy inputs from the magnetosphere can have dramatic effects to the upper atmospheric environment. One of such effects is the changes in ionospheric electron density that can perturb communication and navigation systems.

In this paper, we present the first comparison between the thermosphere-ionosphere electrodynamic general circulation model (TIE-GCM) simulations and the global GPS-GIM observations of TEC during the period of October 18-19, 1995, when an interplanetary magnetic cloud was encountered by the Earth [*Lepping et al.*, 1997] and caused significant geomagnetic disturbances. Figure 1 shows the distribution of the *AE* and D_{st} indices during the 2-day period. A storm sudden commencement (SSC) occurred at about 1100 UT on October 18 due to the impinging of the interplanetary shock in front of the magnetic cloud. The magnetic cloud arrived at the Earth's magnetopause at about 1950 UT on October 18 and lasted for about 30 hrs as the interplanetary magnetic field gradually rotated from strongly southward to strongly northward. It consequently induced a major magnetic storm as well as massive substorms, as indicated by the variations in the *AE* and D_{st} indices. At about 2330 UT on October 18 both D_{st} and *AE* reached their maximum magnitudes, with D_{st} = -120 nT and *AE* = *1600* nT. The different storm phases were identified according to the distribution of D_{st}. In particular, the time interval between 2000 and 2300 UT on October 18 was the main phase of the storm when D_{st} decreased sharply. After 2300 UT, it was

the recovery phase as D_{st} gradually returned to its regular value in next 24 hrs. Note that there were still significant substorm activities during the early part of the storm recovery phase.

TIE-GCM/GPS-GIM comparison

For this particular study we have used the realistic time-dependent high-latitude ionospheric convection and auroral precipitation patterns derived from the assimilative mapping of ionospheric electrodynamics (AMIE) procedure as the inputs to the TIE-GCM *[Richmond et al., 1992].* The 5-min AMIE patterns in both northern and southern hemispheres are derived by fitting the observations from the DMSP F12 and F13, NOAA 12 and 13 satellites, 7 SuperDARN radars, and 116 ground magnetometers over the world (see *Richmond and Kamide [1988], Lu et al. [1996],* and *Emery et al. [1996]* for the fitting procedure.) A 5-min time step is used for the entire 2-day simulation, and the TIEGCM history volumes are recorded every 10 min. In addition to the ionospheric inputs from AMIE, The TIEGCM also requires the inputs of upward propagating semidiurnal and diurnal tides at the lower boundary and solar EUV and UV fluxes at the upper boundary. For the period of October 18-19, 1995, the 2-day average solar radiation index S_a is *80x* 10^{-22} W/m^2Hz. The TIEGCM has an effective 50 latitude-longitude geographic grid with 29 constant pressure levels (from ZP=-7 to ZP=+7 at every one half scale height), extending from about 95 to 600 km. This extension was made to give a better representation for total electron content (TEC). The chemistry treatment in the TIE-GCM has been discussed by *Roble [* 1995].

The global GPS network, overseen by the International GPS Service (IGS) for Geodynamics, contains more than 80 ground-based stations in the October of 1995. Each station is capable of receiving the dual frequency GPS signals from 8 to 12 satellites (24 in total) in different directions simultaneously. As the satellites orbit at about 20,200 km altitude, observations of line-of-sight

TEC, derived from the dual frequency phase and range data, can be made with a fairly good spatial coverage within 15 minutes. Using the techniques developed at the Jet Propulsion Laboratory [*Wilson et al., 1995; Ho et al., 1996; Mannucci et al., 1997],* interpolated global ionospheric maps (GIM) of vertical TEC are obtained every 15 reins over uniformly sized triangular tiles that tessellate the sphere (the three vertices of each tile are separated by about 800 km). The entire mapping is conducted in a Sun-fixed (or local time) geomagnetic coordinate system. Such a reference frame allows updating the LT-Latitude grid points with measurements as each Earth-fixed station rotates by. The magnetic frame is chosen to reduce interpolation errors in consideration of the ionospheric dynamical effects that are largely ordered by the geomagnetic field. The techniques have been proven very effective for mapping sparsely distributed data. It should be noted that the mapping involves the slant-to-vertical TEC conversion as well as spatial and temporal interpolation, which in general may cause certain degradation of the map accuracy with distance away from GPS receivers.

In this study we focus on the relative variations in TEC at high latitudes with respect to a quiet period. For TIE-GCM, the quiet period is the 24-hour background run using the ionospheric inputs at 0000 UT on October 18 (which corresponds to a relatively quiet geomagnetic condition) but adjusted to local time and magnetic latitude as the Earth rotates. For GPS-GIM, the quiet pattern is obtained by a 4-day average of the global TEC maps prior to the storm (October 14-17),

Figures 2 and 3 show the polar maps of TEC difference (with respect to the corresponding quiet-day background) at 2200 UT on October 18 (during the main phase of the storm) and at 0400 UT on October 19 (during the recovery phase of the storm), respectively. In each figure, the TIE-GCM results are shown on the left and the GPS-GIM observations on the right. At the main phase of the storm, both hemispheres show an increase in TEC over the nightside auroral zone.

Such an increase is attributed to the enhancement of auroral precipitation that increases the ionization rate. Note that the auroral oval is slightly shifted toward the duskside in the northern hemisphere, and toward the dawnside in the southern hemisphere. This is due to the offset of the geomagnetic poles from the geographic poles. Considering that the TIE-GCM is a global model with a relatively large grid size and that GPS-GIM has its own observational limitations of spatial coverage, the agreement between the TIE-GCM simulations and the GPS-GIM maps is remarkably good in terms of general distributions of TEC changes. But there are some subtle quantitative differences between the two methods. For instance, the TIE-GCM shows the auroral-zone TEC enhancement extending into northern Russia as well as over Antarctic in the post-midnight sector, while such an enhancement is not that obvious in GPS-GIM which may be due to the lack of stations in those regions. In addition, GPS-GIM tends to have a stronger dayside TEC increase than the TIE-GCM does. During the recovery phase (Figure 3), the increase of TEC remains about the same in the northern auroral zone. In the southern auroral zone, however, the overall TEC is reduced. A main depletion area of TEC can be seen in the auroral-subauroral zone in the southern hemisphere, which extends between 1500 and 2300 LT (there are two depletion regions in GPS-GIM that cover almost the entire duskside auroral zone). A similar depletion also exists in the northern subauroral zone, but within a smaller local-time expansion (between 0700 and 1200 LT) and at lower magnetic latitudes. The northern-southern asymmetry will be discussed in more detail below.

Figure 4 presents the hemispheric integrals of auroral precipitation of energetic electrons (top pane]), the percent difference of total electron content from TIE-GCM (middle panel), and the percent difference of total electron content from GPS-GIM (bottom panel), respectively. Auroral precipitation is derived from AMIE as the energy input to TIE-GCM. The integration is made

above 150° I magnetic latitude to account for the variations within the auroral zones. Solid lines are for the northern hemisphere and dashed lines for the southern hemisphere. There is a good correlation between the enhancement of aurora] precipitation and the increase in total electrons in the northern hemisphere. In the southern hemisphere, however, the total electrons increase as auroral precipitation increases only on October 18 (e.g., during pre-storm as well as the main phase of the storm) but decreases during the recovery phase on October 19, forming an overall negative storm effect in the southern hemisphere.

The asymmetry in total electron variations between northern and southern hemisphere during the recovery phase is a very interesting feature of this event, and it is worthy of further investigation. Figure 5 shows the TIE-GCM difference plots of electron density (with respect to the corresponding quiet-time background) at two selected pressure levels (ZP=-4 and ZP=2) that represent the E- and F-region, respective] y, in the northern and southern hemispheres at 0400 UT on October 19. At ZP=-4 (and below about 200 km), the increase of electron density is well confined to the auroral zone as a result of enhanced ionization caused by auroral precipitation. At ZP=2 (and between about 200 and 500 km), the increase of electron density in the northern aurora] zone diminishes, while a large electron depletion area evolves at subauroral latitudes between 0700 and 1200 LT. In the southern hemisphere, nearly the entire polar region is overwhelmed by electron depletion above 200 km. Comparing with the TEC difference plots shown in Figure 3, it is clear that the change in TEC is the combination of two effects that occur at two altitude ranges: the enhancement in TEC over the aurora] zones corresponds to the electron density increase in the E and lower F regions (below 200 km), and the depletion in TEC is associated with the electron density decrease in the upper F region (above 200 km).

To further examine the cause of electron depletion, the difference plots for the N_2/O ratio at

the same pressure levels are also displayed in Figure 5. 1[appears that, above 200 km, the area of electron density depletion corresponds to the region where $N_2/0$ ratio increases. Similar increase in 0_2 and N_2 densities (not shown) are found in the F-region as well. Such correlation between electron density depletion and molecular density increase is not surprising since the increased 0_2 and N_2 would result in increased conversion of 0^+ to O_2^+ and NO+, which rapidly recombine with electrons to decrease the electron density [*Rishbeth*, 1989; *Burns et* al., 199 S]. In the E region below 200 km, the simulation shows no apparent correlation between the electron and molecular density distributions.

It should be pointed out that both the total hemisphere-integrated Joule heating and auroral precipitation are about the same in the two hemispheres during the 2-day period. The asymmetry between the northern and southern hemispheres therefore cannot be simply explained by the different magnetospheric energy inputs. To explore the possible cause for the hemispheric asymmetry, we show in Figure 6 the difference plots for the N_2/O ratio at the pressure level ZP=3 at 2200 UT on October 18 and at 0400 UT on October 19, respective] y. The asterisks indicate the magnetic poles. At 2200 UT (the main phase of the storm), the increase in $N_2/0$ is primarily located in the early morning auroral zones. As time proceeds, the $N_2/0$ bulges in both hemispheres tend to move toward dayside due to coronation. In addition to that, the enhancement in $N_2/0$ also expands into the entire nightside auroral zone in the southern hemisphere. This is probably due to the fact that, from 2200 to 0400 UT, the magnetic south pole is moving toward the daysidc so that the southern hemisphere becomes more summer-like (the terminator of the sunlight is about 20° nightside of the dawn-dusk magnetic meridian). The normal upward motions in the sunlit ionosphere help enrich the $N_2/0$ ratio, so that the storm-time augmentation of that upward motion by

Joule heating can more readily enhance the high-latitude N_2/O ratio. In (he northern hemisphere, by contrast, the magnetic pole is moving away from the Sun so that it is more winter-like (the terminator of the sunlight is about 25° dayside of the dawn-dusk magnetic meridian). To what extent this universal-time effect in the peculiar hemispheric asymmetry may be primarily a phenomenon of the storm recovery phase remains to be determined by future studies.

Summary

The global observations of TEC from GPS ground receivers have provided a unique opportunity to test the ability of the NCAR TIE-GCM to simulate the upper atmospheric response to geophysical disturbances during the October 1995 Space Weather event. This study has shown that, using realistic magnetospheric inputs, TIE-GCM is able to capture the main features in thermospheric/ionospheric variations. The agreement between the TIE-GCM simulations and the GPS-GIM measurements is remarkably good.

We have shown in this study that the changes in total electron content are the combination of very different variations at different altitudes, with electron density enhancement at lower altitude (due to auroral precipitation) and depletion at higher altitude (clue to molecular density increase). A hemispheric asymmetry in total electrons during the storm recovery phase is found in both model simulations and GPS-GIM observations, that appears to be linked to the asymmetric solar heating, analogous to the well-known seasonal variations of ionospheric storms [e.g., *Fuller-Rowell et al.*, 1997, and references therein].

Acknowledgments. We thank the GEM community for providing various data that have used to drive both AMIE and TIE-GCM for this study, and we are grateful to the institutions that support

the IGS GPS network, and to the GPS Networks and Ionospheric Systems Development group at the Jet Propulsion Laboratory for the development of GIM that made this study possible. We are indebted to B. Foster, C. Ridley, and B. Emery for their effects in developing the TIE-GCM processors and plotting programs. Work at HAO/NCAR was supported in part by the NFS Space Weather grant and by the NASA Space Physics Theory Program. Work at JPL was under a contract with the National Aeronautics and Space Administration.

References

Burns, A. G., T. L. Killeen, G. R. Carignan, and R. G. Roble, Large enhancements in the O/N2 ratio in the evening sector of the winter hemisphere during geomagnetic storms, *J. Geophys. Res.*, 100, 14,661, 1995

Emery, B. A., et al., Assimilative mapping of ionospheric electrodynamics in the thermospheric-ionospheric general circulation model comparisons with global ionospheric and thermospheric observations during the GEM/SUNDIAL period of March 28-29, 1992, *J. Geophys. Res.*, *101,26,681,* 1996.

Fuller-Rowell, T. J., M. V. Codrescu, R. G. Roble, and A. D. Richmond, How does the thermosphere and ionosphere react to a geomagnetic storm? in *Magnetic Storms,* Geophysical Monograph 98, AGU, 203, 1997.

Ho., C. M., A. J. Mannucci, U. J. Lindqwister, *X.* Pi, B. Tsurutani, Global ionospheric perturbations monitored by the worldwide GPS network, *Geophys. Res. Lett.*, 23, 3219, 1996.

Lepping, R. P., et al., The WIND magnetic cloud and events of October 18-20, 1995: Interplanetary properties and as triggers for geomagnetic activity, *J. Geophys. Res.*, 102, 14,049, 1997.

Lu, G., et al., High-latitude ionospheric electrodynamics as determined by the assimilative map-

ping of ionospheric electrodynamics procedure for the conjunctive SUNDIAL/ATLAS 1/ GEM period of March 28-29, 1992, *J. Geophys. Res.*, *101*, 26,697, 1996.

Mannucci, A. J., B. D. Wilson, D. N. Yuan, C. M. Ho, U. J. Lindqwister, T. F. Runge, A global mapping technique for GPS-derived ionospheric TEC measurements, *Radio Sci.*, in press, 1997.

Richmond, A. D., E. C. Ridley, and R. G. Roble, A thermosphere/ionosphere general circulation model with coupled electrodynamics, *Geophys. Res. Lett.*, *19*, 601, 1992.

Richmond, A. D., and Y. Kamide, Mapping electrodynamics features of the high-latitude ionosphere from localized observations: Technique, *J. Geophys. Res.*, *931*, 5741, 1988.

Rishbeth, H., F-region storms and thermospheric composition, in Electromagnetic Coupling in the Polar Clefts and Cusps, Eds., P. E. Sandholt and A. Egeland, pp. 393, 1989.

Roble, R. G., Energetic of the Mesosphere and Thermosphere, in *The Upper Mesosphere and Lower Thermosphere: A Review of Experiment and Theory,* Geophysical Monograph 87, AGU, 1-21, 1995.

Wilson, B. D., A. J. Mannucci, C. D. Edwards, Subdaily northern-hemisphere maps using an extensive network of GPS receivers, *Radio Sci.*, 30., 639,1995.

Figure Captions

Figure 1. Distributions of *AE* and D_{st} indices during the period of October 18-19, 1995.

Figure 2. Polar maps of changes in total electron content (left) derived from TIE-GCM (above 142.5° I geographic latitude) and (right) from GPS-GIM (above 140° I geographic latitude) during the main phase of the storm at 2200 UT on October 18, 1995. The GPS ground stations are indi-

cated by the white dots. The color scale represents the changes in TEC units (10^{12} electrons/cm^2)

Figure 3. Similar to Figure 2, but during the recovery phase of the storm at 0400 UT on October 19.1995.

Figure 4. Hemispheric integrals of (a) auroral precipitation, (b) percent difference of total electron content from the TIE-GCM, and (c) percent difference of total electron content from GPS-GIM. Solid lines are for the northern hemisphere, and dashed lines for the southern hemisphere.

Figure 5. Changes in electron density and $N_2/0$ ratio at selected pressure levels at 0400 UT on October 19, 1995. The contour interval is 2.5x104 cm^{-3} for electron density. For the $N_2/0$ ratio, the contour interval is 1 at ZP=-4 and 0.1 at ZP=2.

Figure 6. Changes in $N_2/0$ ratio (left) at 2200 UT on October 18 and (right) at 0400 UT on October 19, 1995. The northern hemisphere is on the top, and the southern hemisphere on the bottom.

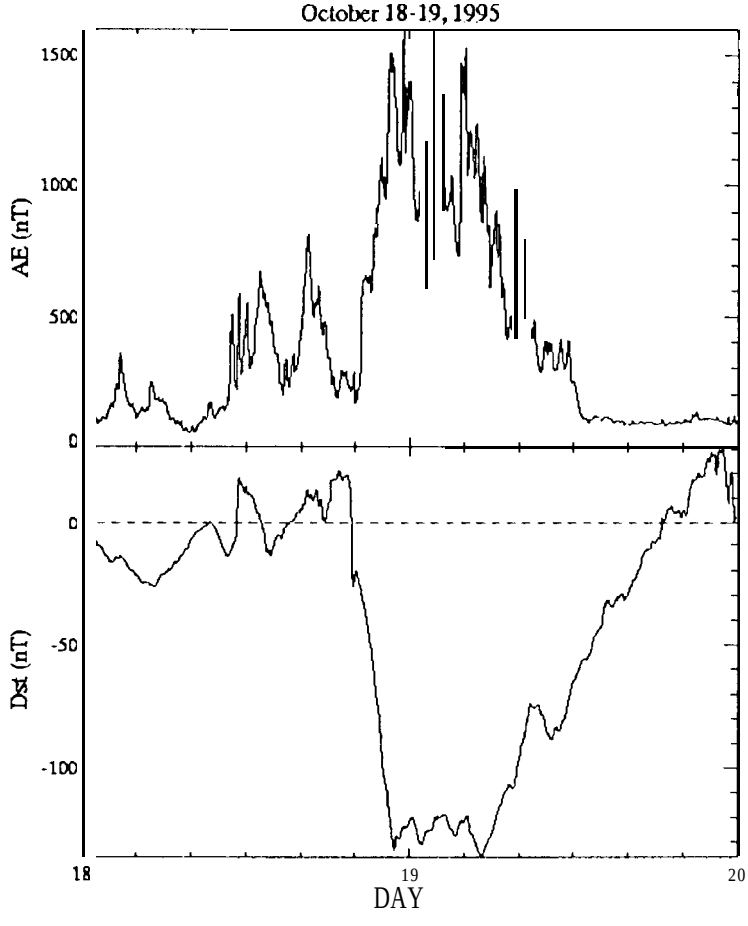
October 18-19, 1995
1500
1000
500
0
AE (nT)
0
-50
-100
Dst (nT)
18
19
20
DAY

Fig 1

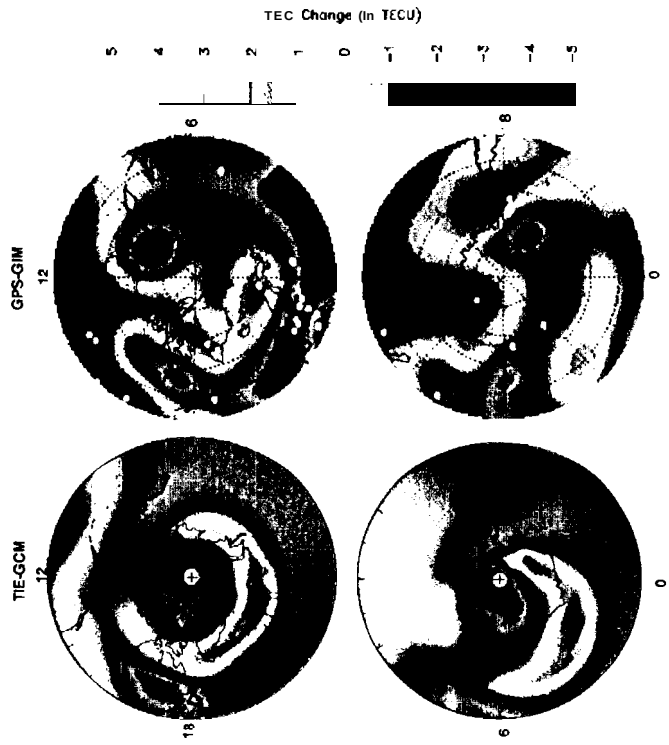

Fig 2

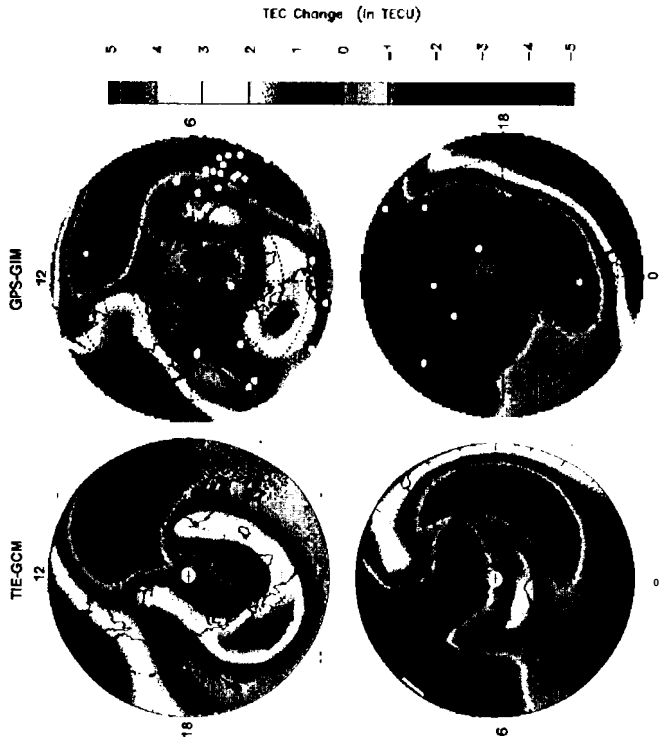

Fig 3

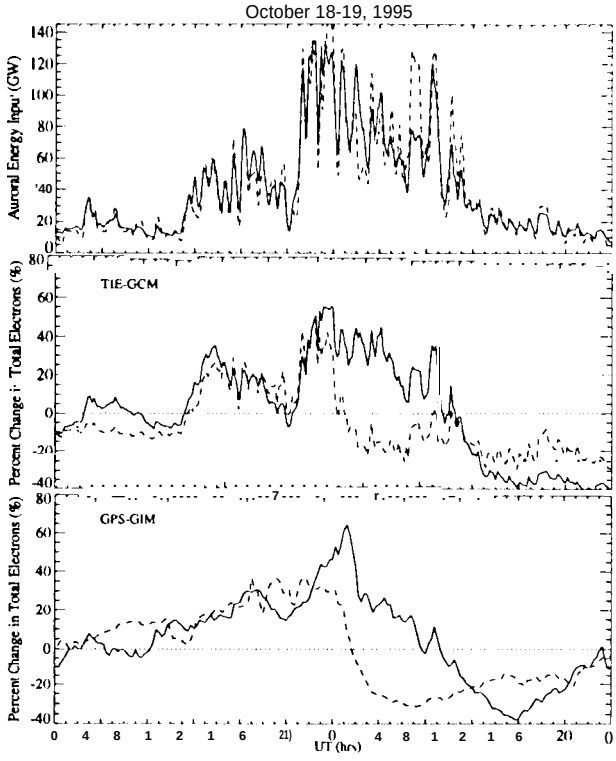
October 18-19, 1995
Auroral Energy Input (GW)
Percent Change in Total Electrons (%)
TIE-GCM
GPS-GIM
UT (hrs)

Fig 4.

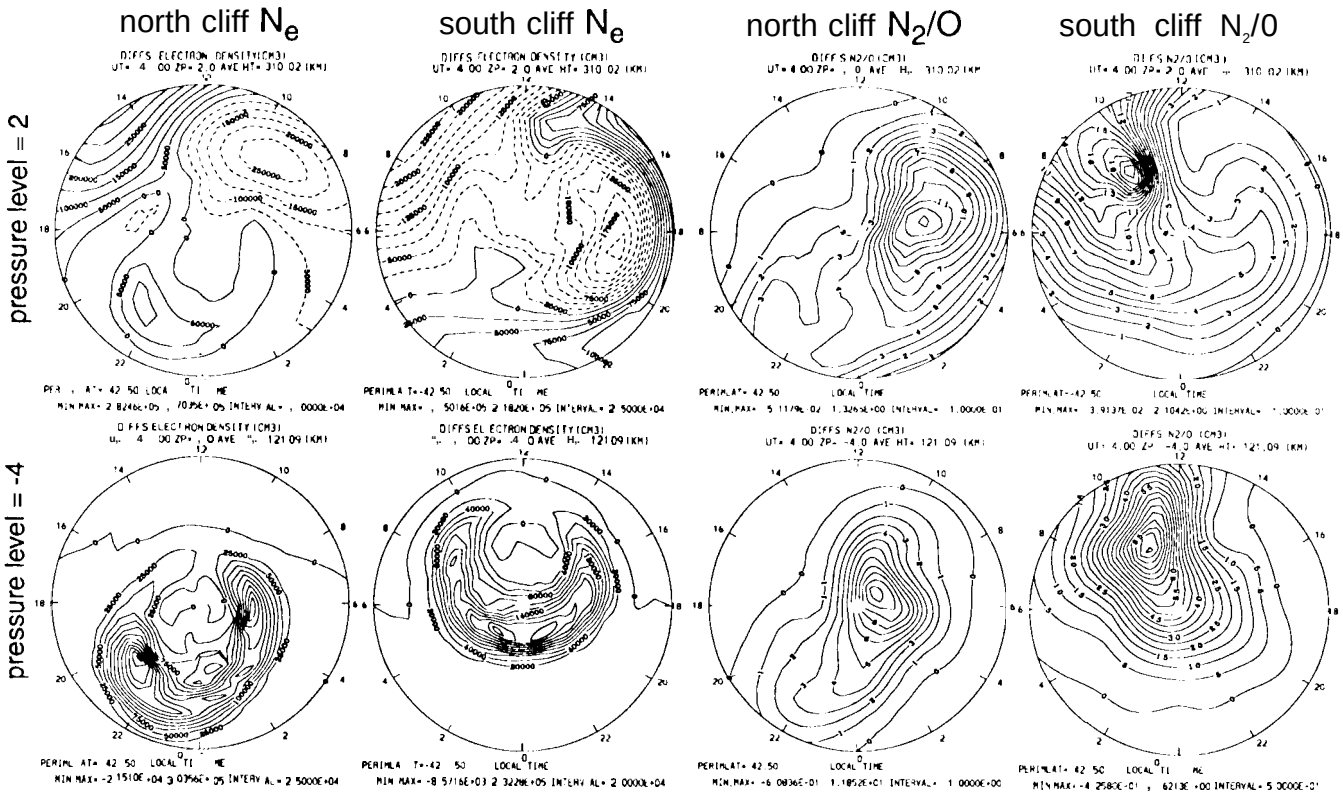
north cliff N_e
south cliff N_e
north cliff N_2/O
south cliff N_2/O
pressure level = 2
pressure level = -4

Fig 5

10/18 22:00 UT

10/19 04:00 UT

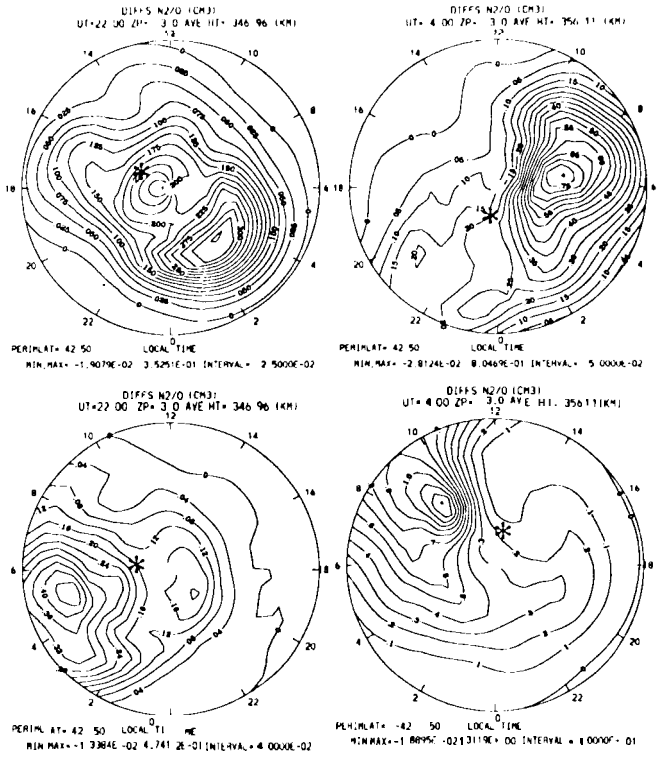

Fig 6